

**Supplementary on-line information for****A synthetic gene-metabolic oscillator**

Eileen Fung<sup>1,2</sup>, Wilson W. Wong<sup>1</sup>, Jason K. Suen<sup>1</sup>, Thomas Bulter<sup>1</sup>, Sun-gu Lee<sup>1</sup>, and James C. Liao<sup>1,2</sup>

<sup>1</sup>*Department of Chemical Engineering, <sup>2</sup>Biomedical Engineering Interdepartmental Program, University of California-Los Angeles, Los Angeles, CA 90095*

**1. Modeling, simulation, and analysis of the Metabolator:**

The design of the metabolator is aided by an ODE-based model that describes the key components of the system. The dynamic balance of the metabolites (AcCoA, AcP, OAc<sup>-</sup>, and HOAc) are given by:

$$\begin{aligned} \frac{d \text{AcCoA}}{dt} &= V_{\text{Acs}} - V_{\text{Pta}} + V_{\text{gly}} - V_{\text{TCA}} \\ \frac{d \text{AcP}}{dt} &= V_{\text{Pta}} - V_{\text{Ack}} \\ \frac{d \text{OAc}^-}{dt} &= V_{\text{Ack}} - V_{\text{AcE}} - V_{\text{Acs}} \\ \frac{d \text{HOAc}}{dt} &= V_{\text{AcE}} - V_{\text{out}} \end{aligned}, \quad (\text{S1})$$

where  $V_i$  are the reaction rate expressions defined in Table S1. The glycolytic rate is treated as a constant. The flux to the TCA cycle and EtOH and the export flux of HOAc are assumed first order with respect to AcCoA and HOAc, respectively. The Michaelis-Menten rate law is used to describe Pta, Ack, and Acs enzyme kinetics (see Table S1).

The concentrations of the three key proteins LacI, Pta, and Acs are determined by

$$\begin{aligned} \frac{d}{dt} \text{LacI} &= R_{\text{LacI}} - R_{d,\text{LacI}} \\ \frac{d}{dt} \text{Pta} &= R_{\text{Pta}} - R_{d,\text{Pta}} \\ \frac{d}{dt} \text{Acs} &= R_{\text{Acs}} - R_{d,\text{Acs}} \end{aligned}, \quad (\text{S2})$$

where  $R$ 's represent the synthesis and degradation rates of the proteins, which are also defined in Table S1. Transcription and translation are lumped into protein synthesis rates, which are described by the Hill kinetics with a constant basal expression rate. The synthesis rates reflect promoter activity modulated by

either AcP or LacI. The degradation is assumed first order kinetics. Note that the dilution due to cell growth is also first order and can be lumped into the first-order term in each equation in Eqs. S1 and S2 for simplicity.

Numerical analysis of the resulting model was conducted in two parts. First, we used the 4<sup>th</sup> order Runge-Kutta integration to explore the nonlinear dynamics of the system described by Eqs S1 & S2<sup>1</sup>. Fig. 3a shows a sample simulation which demonstrates that an increase in the glycolytic rate destabilizes the steady state and leads into a sustained periodic state. The exact parameter values used in this simulation are shown in Table S1. Next, the stability of the steady state solution of the metabolator model (Eqns S1 and S2) is examined by using linear stability analysis<sup>2,3</sup>. We are particularly interested in the Hopf bifurcation, which characterize the transition from the steady state solution to a periodic state at criticality. The onset of the Hopf bifurcation is determined at the moment when the real part of a complex conjugate pair of eigenvalues of the Jacobian matrix crosses zero, while the real parts of all other eigenvalues remain negative. We are interested in constructing phase diagrams by mapping the locus of Hopf bifurcation (the boundary where the real part of pairs is exactly zero) as functions of key parameters such as acetate concentration, glycolytic rate, and maximum synthesis rates of proteins. To do so, we compute the response of the steady state solution (base state) to infinitesimal perturbations by solution of the system linearized about the same steady state. This linear response is determined by calculation of the eigenvalues in the linear spectrum that have the largest real part,  $\sigma$ . The critical point for the Hopf bifurcation is then computed by interpolating for the parameter that corresponds to  $\sigma = 0$ . Repeating the same process for different sets of parameters generates the phase diagram, such as the ones shown in Fig. 3b & c.

**Reference:**

1. B.A. Finlayson. *Nonlinear Analysis in Chemical Engineering*, (Mcgraw-Hill College, New York, 1980).
2. G. Iooss and D.D. Joseph, *Elementary Stability and Bifurcation Theory*, (Springer-Verlag, New York, 1989).
3. J. Guckenheimer and P. Holmes, *Nonlinear Oscillations, Dynamical Systems, and Bifurcations of Vector Fields*. (Springer-Verlag, New York, 1983).

**Table S1. Rate expressions used in Eqs. S1 & S2 and values used for the dimensionless parameters in Figs 3a–d.**

|  | Rate expression   | Parameters in Fig. 3a,b                                    | Parameters in Fig. 3c      | Parameters in Fig. 3d                      |
|--|---|--|----------------------------|--|
| Glycolytic flux, $V_{\text{gly}}$  | $V_{\text{gly}} = S_0$  | $S_0 = 0.001 \dots 0.5$ (a)<br>$S_0 = 1$ (b)               | $S_0 = 10^{-4} \dots 10^4$ | $S_0 = 10$                                 |
| Flux to TCA cycle and EtOH production, $V_{\text{TCA}}$  | $V_{\text{TCA}} = k_{\text{TCA}} \text{AcCoA}$  | $k_{\text{TCA}} = 10$                                      |                            |  |
| Pta flux, $V_{\text{Pta}}$   | $V_{\text{Pta}} = \frac{k_1 \text{Pta} \cdot \text{AcCoA}}{(K_{m,1} + \text{AcCoA})}$             | $k_1 = 80, K_{m,1} = 0.06^1$                               |                            |  |
| Acs flux, $V_{\text{Acs}}$   | $V_{\text{Acs}} = \frac{k_2 \text{Acs} \cdot \text{OAc}^-}{(K_{m,2} + \text{OAc}^-)}$             | $k_2 = 0.8, K_{m,2} = 0.1^1$                               |                            |  |
| Flux for the reaction $\text{AcP} \xrightleftharpoons{\text{Ack}} \text{OAc}^-$ , $V_{\text{ack}}$ | $k_{\text{Ack},f} \text{AcP} - k_{\text{Ack},r} \text{OAc}^-$                                     | $k_{\text{Ack},f} = 1, k_{\text{Ack},r} = 1$               |                            |  |
| Acid-base equilibrium for acetic acid, $V_{\text{Ace}}$  | $C(\text{AcP} \cdot \text{H}^+ - K_{\text{eq}} \text{OAc}^-)$                                     | $C = 100, \text{H}^+ = 10^{-7}, K_{\text{eq}} = 10^{-4.5}$ |                            |  |
| HOAc intercellular transport rate, $V_{\text{out}}$  | $V_{\text{out}} = k_3 (\text{HOAc} - \text{HOAc}_E)$  | $k_3 = 0.01$   | $\text{HOAc}_E = 0$        | $\text{HOAc}_E = 0 \dots 30$               |
|  |   |  | $\text{HOAc}_E = 0$        | $\text{HOAc}_E = 0$                        |
| LacI synthesis rate, $R_{\text{LacI}}$   | $R_{\text{LacI}} = \frac{\alpha_1 (\text{AcP}/K_{g,1})^n}{1 + (\text{AcP}/K_{g,1})^n} + \alpha_0$ | $\alpha_1 = 0.1, K_{g,3} = 10, n = 2, \alpha_0 = 0$        |                            |  |
| Acs synthesis rate, $R_{\text{Acs}}$   | $R_{\text{Acs}} = \frac{\alpha_2 (\text{AcP}/K_{g,2})^n}{1 + (\text{AcP}/K_{g,2})^n} + \alpha_0$  | $K_{g,2} = 10, n = 2, \alpha_0 = 0$                        |                            |  |
|  |   | $\alpha_2 = 20 \cdot \alpha_1 = 2$                         |                            | $\alpha_2 = (0 \dots 30) \cdot \alpha_1$   |
| Pta synthesis rate, $R_{\text{Pta}}$   | $R_{\text{Pta}} = \frac{\alpha_3}{1 + (\text{LacI}/K_{g,3})^n} + \alpha_0$                        | $K_{g,3} = 0.001, n = 2, \alpha_0 = 0$                     |                            |  |
|  |   | $\alpha_3 = 20 \cdot \alpha_1 = 2$                         |                            | $\alpha_3 = (0 \dots 10^5) \cdot \alpha_1$ |
| Degradation rate, $R_{d,X}$ ( $X = \text{LacI}, \text{Acs}, \text{Pta}$ )                          | $R_{d,X} = k_d X$   | $k_d = 0.06$   |                            |  |

<sup>1</sup> BRENDA. <http://www.brenda.uni-koeln.de/index.php4>

## 2. On the consistent dynamics between GFP reporting and underlying dynamics of the metabolator

Consider an ODE model for the green fluorescence protein (GFP) dynamics where the GFP degradation is modelled by a first order reaction kinetics,

$$\frac{d \text{GFP}(t)}{dt} = R_{\text{GFP}}(x(t)) - k_d \text{GFP}(t), \quad (\text{S3})$$

where  $R_{\text{GFP}}(x(t))$  is the synthesis rate of GFP,  $x(t)$  is the species that activate or repress GFP, and  $k_d$  is the degradation rate constant. Rearranging S3 yields,

$$\frac{d \text{GFP}(t)}{dt} + k_d \text{GFP}(t) = R_{\text{GFP}}(x(t)), \quad (\text{S4})$$

and the analytical solution with an appropriate initial condition yields,

$$\text{GFP}(t) = \int_{t_0}^t e^{-k_d(t-s)} R_{\text{GFP}}(x(s)) ds. \quad (\text{S5})$$

Let an arbitrary synthesis rate of GFP,  $R_{\text{GFP}}(x(t))$ , be represented by a discrete Fourier series,

$$R_{\text{GFP}}(x(t)) = m + \sum_n A_n \cos \omega_n t + B_n \sin \omega_n t, \quad (\text{S6})$$

where  $\omega_n$  is the frequency component of the dynamics of synthesis rate, and  $m$  be the baseline synthesis rate. Analytical evaluation of Eqn. S5 for GFP dynamics yields,

$$\text{GFP}(t) = \frac{m}{k_d} + \sum_n \frac{1}{k_d^2 + \omega_n^2} [(k_d A_n - \omega_n B_n) \cos \omega_n t + (\omega_n A_n + k_d B_n) \sin \omega_n t] - D_1 e^{-k_d(t-t_0)}, \quad (\text{S7})$$

Where

$$D_1 = \frac{m}{k_d} + \sum_n \frac{1}{k_d^2 + \omega_n^2} [(k_d A_n - \omega_n B_n) \cos \omega_n t_0 + (\omega_n A_n + k_d B_n) \sin \omega_n t_0]. \quad (\text{S8})$$

If there exists a single dominant frequency in the  $R_{\text{GFP}}(x(t))$  dynamics such that

$$R_{\text{GFP}}(x(t)) = m + A \cos \omega t + B \sin \omega t, \quad (\text{S8})$$

then the corresponding GFP dynamics becomes,

$$\text{GFP}(t) = \frac{m}{k_d} + \frac{1}{k_d^2 + \omega^2} [(k_d A - \omega B) \cos \omega t + (\omega A + k_d B) \sin \omega t] - D_1 e^{-k_d(t-t_0)}, \quad (\text{S9})$$

where,

$$D_1 = \frac{m}{k_d} + \frac{1}{k_d^2 + \omega^2} [(k_d A - \omega B) \cos \omega t_0 + (\omega A + k_d B) \sin \omega t_0]. \quad (\text{S10})$$

When compared with the synthesis rate (Eqn. S8),  $R_{\text{GFP}}(x(t))$ , the degradation rate constant of GFP may affect the amplitude of oscillation but not the period of the oscillation. This suggests that the oscillation period observed in the single cell experiment is consistent with the underlying dynamics of the metabolator. On the other hand, the GFP dynamics displays a phase shift and changes in amplitude that depends on the relative magnitude between the oscillation period of  $R_{\text{GFP}}(x(t))$  and the degradation rate constant. If the frequency of oscillation is much greater than the degradation rate constant, then the amplitude of the GFP oscillation is invariant from changes in degradation rate constant. In the metabolator construction, the degradation tag on GFP has a half life that is three times larger than that of the oscillation period of the metabolator. Therefore, the oscillation frequency is larger than the degradation rate of GFP and the oscillation frequency of GFP should be independent of the degradation.

We further test the hypothesis of the oscillation period recorded by GFP dynamics to be consistent with the underlying oscillation of the metabolator numerically. Such model is constructed by coupling Eqns S1, S2, and S3 together. Numerical simulation is conducted by using the fourth order Runge-Kutta algorithm. Three different values of the degradation rate constant,  $k_{d,\text{GFP}}/k_{d,\text{Pta}} = 0.1, 1, 10$ , are used in the simulation. The period obtained for the GFP dynamics is 40 units, which is the same as the underlying oscillation dynamics of the metabolator model. The amplitude of the GFP dynamics does not change with the degradation rate constant. This is consistent with the numerical solution where  $k_d \ll T$ , where  $T$  is the period of oscillation. These simulation results, coupled with the analytical result shown in Eqn. S9, suggest that the oscillation period of observed dynamics by GFP is consistent with the underlying dynamics of the metabolator.

### 3. On the stability of limit cycle oscillation exhibited by the metabolator model

We demonstrated that the oscillation dynamics of the metabolator model (Eqns S1 and S2) are limit cycles (Fig 3a, b). In this section, we further examine the stability of the limit cycle oscillation by using Floquet analysis<sup>1</sup>. Specifically, we compute the eigenvalues of the monodromy matrix,  $\mathbf{M}$ , defined as  $\mathbf{M} \equiv \Phi(T)$ , where  $T$  is the period of the limit cycle oscillation, and  $\Phi(t)$  is the solution of the matrix initial value problem,

$$\frac{d\Phi}{dt} = \mathbf{J}(\mathbf{x}(t)) \cdot \Phi, \quad (\text{S10})$$

with initial condition of  $\Phi(0) = \mathbf{I}$ . In Eqn. S10,  $\mathbf{J}(\mathbf{x}(t))$  is the Jacobian matrix of the ODE model (Eqns S1 and S2) evaluated at the instantaneous value of the oscillatory motion of the nonlinear ODE model. In other words, Eqn. S10 is a matrix-valued ODE with time periodic coefficient. The eigenvalues of the monodromy matrix  $\mathbf{M}$  consists of the key information of the periodic state. A periodic state is stable if there exists one eigenvalue equals to +1 and all other eigenvalues have modulus less than unity  $|\mu_n| < 1$ . We examine the stability of the limit cycle for  $V_{gly} = 0.5$  and  $V_{gly} = 1$ . All the eigenvalues for both cases are real. The set of eigenvalues for  $V_{gly} = 0.5$  is  $[0.9998, 0.5751, 0.06579, 0, 0, 0.05972, 0.05972]$  and that for  $V_{gly} = 1$  is  $[1.000, 0.7258, 0.6252, 0.09140, 0.004102, 0, 0]$ . This suggests that the limit cycle may lose stability to another limit cycle at even higher glycolytic rate as the value of the second eigenvalue increases towards +1 as  $V_{gly}$  increases. We did not investigate the stability of this limit cycle further because the glycolytic rate for the instability to occur may be irrelevant for explaining or describing the metabolator dynamics. In the same spirit, we note that there may be additional nonlinear dynamics occurring with the ODE model that corresponds to region that are not relevant for our discussion.

#### Reference:

1. G. Iooss and D.D. Joseph, *Elementary Stability and Bifurcation Theory*, (Springer-Verlag, New York, 1989).

## 4. Stochasticity of regulatory control induces variations amplitude of oscillation by the metabolator

The nonlinear ODE model for the metabolator (Eqn. S1 and S2) makes use of the continuum assumption. Biomolecular events, especially at the gene regulation level, are highly stochastic and discrete. This stochasticity may account for much of the discrepancy between model prediction and experimental observation. Classical stochastic simulation approaches such as the Gillespie algorithm<sup>1</sup> have been widely applied in biochemical reaction network and have been demonstrated to have substantial influence on the resulting dynamics<sup>2</sup>. In this section, we used a statistically equivalent approach, the Langevin technique, to model the stochastic behavior of the metabolator. This approach provides additional insights to the system behavior<sup>3</sup>. We treat each component of the nonlinear model as continuous variable and add Gaussian white noise to specific parameter in the system to examine the effect of stochasticity on the resulting dynamics<sup>4</sup>. Specifically in this section, we demonstrate the effect of stochasticity on degradation and synthesis of protein on the oscillation amplitude computed by the metabolator model (Eqns S1 and S2).

For a specific parameter  $\lambda$ , we add a fluctuation,  $\xi$ , modelled by a Gaussian process  $\xi \sim N(0, \sigma)$  and impose a constraint such that  $\lambda > 0$  by using a reflecting boundary condition. The resulting stochastic differential equation is then integrated by using the weak Euler's scheme<sup>4</sup>.

We analyzed the effect of the stochasticity in the various gene regulation parameters on the oscillatory dynamics of the nonlinear ODE model. Perturbations on all parameters in the protein synthesis appear to have similar qualitative effect on the resulting dynamics. Fig. S1 compares the dynamics effect of stochasticity on the degradation rate constants for Pta, LacI, and Acs as a function of amount of stochastic noise added to the system. The amplitude of the resulting oscillatory dynamics, represented by the LacI, was substantially affected. This analysis supports our claim that the stochasticity of regulatory control may accounts for the amplitude variation in the oscillatory dynamics exhibited by the metabolator.

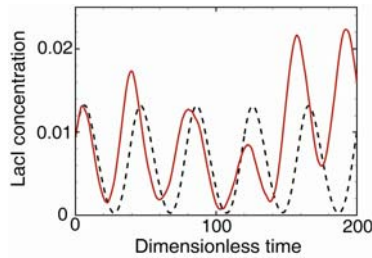


Figure S1. Effect of stochastic noise on the nonlinear dynamics of the metabolator model by using the Langevin approach. The solid line corresponds to the simulation with 10% noise and the dash line corresponds to the simulation without stochastic noise.

**Reference:**

1. Gillespie, D.T. Exact simulation of coupled chemical reactions. *J. Phys. Chem.* **81**, 2340-2361 (1977).
2. Elowitz, M. B. & Leibler, S. A synthetic oscillatory network of transcriptional regulators. *Nature* **403**, 335-338 (2000).
3. Kepler, T.B. & Elston, T.C. Stochasticity in transcriptional regulation: origins, consequences and mathematical representations. *Biophys. J.* **81**, 3116-3136 (2001).
4. Garcia-Ojalvo, J., Elowitz, M. B. & Strogatz, S. H. Modeling a synthetic multicellular clock: Repressilators coupled by quorum sensing. *PNAS* **101**, 10955-10960 (2004).
5. Kloeden P.E. and Platen, E. *Numerical Solution of Stochastic Differential Equations*. (Springer-Verlag, New York, New York, 1992).